Heat transfer enhancement in miniature pipe flows

D. LAKEHAL[1*], C. NARAYANAN[1,2], L. TADRIST[3]

[1]ASCOMP GmbH, Technoparkstrasse 1, H22, 8005 Zurich, Switzerland
[2]Institute of Energy Technology, ETH Zurich, ETH Zentrum 8092 Zurich, Switzerland
[3]IUSTI, Département de Mécanique Energétique, Polytech. Marseille, 13453 Marseille, France
[*](corresponding author: lakehal@ascomp.ch)

Summary - Detailed multi-fluid dynamics simulations have been performed to study two-phase flow and heat transfer in small pipes. Interface tracking methods are shown to be best suited for solving the coupled heat fluid-flow problem, providing detailed information about the physics of the transport processes. The heat removal rate in two-phase flow is higher than in single phase: the bubbly, slug and slug-train patterns transport as much as three-to-four times more heat from the tube wall to the bulk flow than pure water flow. Subtle differences are revealed during the slug to slug-train flow transition.

1. Introduction

Detailed CMFD studies are rare in the context of two-phase flow heat transfer in pipes as compared to experimental investigations, except the contribution of Ua-Arayaporn *et al.* [1] who conducted a similar investigation as the present one, though in a periodic small box rather than in an elongated tube. Their data for heat transfer suffered in turn from domain size effects, and did not allow drawing a clear conclusion as to the real impact of two-phase flow on heat transfer. In this paper we report on the way this class of flow is tackled by use of the Level Set approach [2], in which we have incorporated phase-change [3], and triple-line dynamics modelling capabilities based on the slip-length approach [4]. The focus here is on the role played by flow regime patterns and associated blockage/confinement effects in controlling heat transfer. We will show that slight changes in the inlet flow conditions can trigger flow regime transition from bubbly to slug or slug-train, which in turn leads to an increase in local heat transfer. The 2D axisymmetric simulations were performed in a 1mm diameter tube heated at the surface, in which air and water were injected as co-flowing streams. The computational strategy combines the unsteady Navier-Stokes equations for the flow and Level Sets for interface dynamics. The measurements (for reference) are from [5].

2. Simulation framework

2.1. The TransAT Solver

The CMFD code TransAT© [6,7] is a multi-physics, finite-volume code based on solving the transient multi-fluid Navier-Stokes equations. The code uses structured meshes, though allowing for multiple blocks to be set together. MPI parallel based algorithm is used in connection with multi-blocking. The grid arrangement is collocated and can thus handle more easily curvilinear skewed grids. The solver is pressure based (Projection Type), corrected using the Karki-Patankar technique for compressible flows (up to transonic flows). The code consists of three branches used whenever required: a fully explicit one for LES (3D), and an implicit one for RANS (2D axisymmetric and 3D). High-order time marching and convection schemes can be employed; up to third order Monotone schemes in space. Multiphase flows are tackled using the particle tracking approaches, or interface tracking techniques for both laminar and turbulent flows. The one-fluid formulation context on which TransAT© is built is such that the flow is supposed to evolve in one fluid with variable material properties, which

vary according to the colour function identifying gas and liquid phases. Specifically, we have used for this work the Level-Set approach to track interfaces while advected by the flow [2,3].

2.2. The experiment and CMFD set-ups

The data used for reference in this work are taken from the Chen *et al.*'s experiments [5], which were conducted without heat transfer. In that campaign, air-water flow was pumped at various flow rates in a closed loop into a 1mm diameter pipe. Five flow regimes were investigated: bubbly, slug, bubbly-train slug, churn and annular. The measurements provide the exact void fractions for specific inlet mass flow rates, which help set the computational boundary conditions. The simulations were conducted under axisymmetric conditions in circular horizontal tubes for single and two-phase flow, without gravity. Only the first three flow patterns were investigated. To study the flow-pattern effects on the heat transfer, we have set the pipe wall to a constant temperature (T_w = 340 K), and the inflow to T_{in} = 300 K. The inlet flow conditions were extracted from the experiment, which provided the exact void fraction distribution for each set of superficial liquid and gas velocities. No-slip conditions were applied at the wall. The temperature was taken as a passive scalar, where gravity was ignored. Preliminary grid and domain sensitivity studies have revealed that a domain extension of at least 40 diameters is necessary for the multiphase flows to establish a sort of steady state; 70D for the single phase flow. Various grid resolutions were first tested to assure that the velocity and wall thermal layers are well resolved. Although the intermediate grid of 30 x 600 nodes was sufficient to resolve the macro flow topology and transition (half pipe), grid-dependence study required to increase the resolution in the streamwise direction up to 900. The liquid and gas inflow velocities and corresponding void fractions α are listed in Table 1; the void fractions were set by adjusting the gas inlet area.

Case study	α	U_G	U_L	**Domain size**
	%	*m/s*	*m/s*	*D*
Water	0.0	0.0	1.1	1 X 70
Bubbly	0.205	0.66	1.1	1 X 40
Slug	0.376	0.66	1.1	1 X 40
Bubbly/slug	0.480	1.57	1.1	1 X 40

Table 1: *Inflow velocity and void fraction conditions*

3. Thermal-flow structure: from break-up to steady-state

Figure 1 depicts the simulated flow patterns in the bubbly flow regime. The isocontours refer to the pressure field; the white line indicates the interface. The upper panel of the figure shows the evolution of the flow while the breaking of the initial air jet is taking place. The capsule is elongated by the action of interfacial shear, then breaks at *x/D* = 4 when surface tension effects exceed the shear. Individual bubbles are then released almost periodically. The periodicity of the bubble passage is somewhat disrupted in the second panel, then restored later on at *30D* downstream, as shown in the third panel. This result corroborates to a certain extent with Chen *et al.*'s experiments. Figure 2 shows the slug detachment from the initial flow break-up, which takes place now further downstream as compared to the bubbly flow; i.e. at *x/D* = 7. Surface tension effects dominate the shear actions at a later position as compared to the bubbly flow. Like in the previous scenario, the break-up is in essence a stability phenomenon, in which surface tension, inertia and shear are simultaneously in work. The simulations compare pretty well with experiments [5]. The figure reveals the strong interaction between the slug and the wall, a proximity that is shown later to be responsible for substantial heat transport down to the core-flow region.

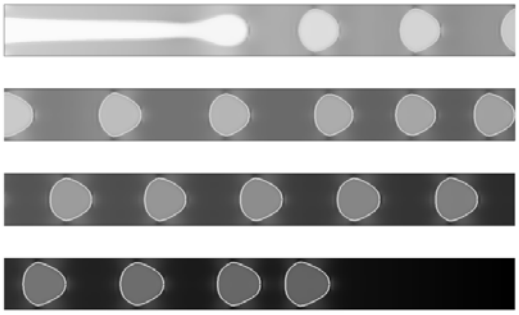

Figure 1: *Bubbly flow formation and evolution*

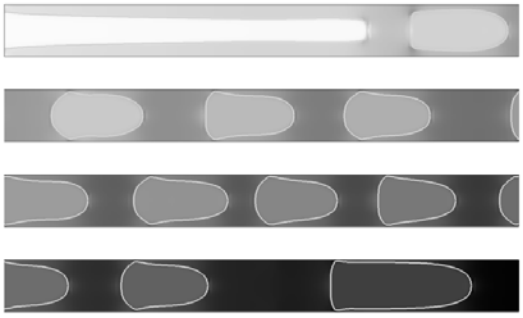

Figure 2: *Slug flow formation and evolution*

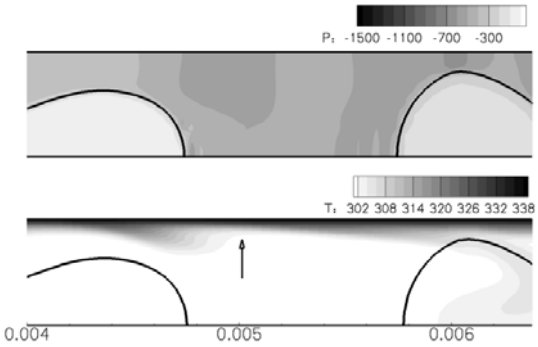

Figure 3: *Pressure and temperature isocontours at break-up point in the bubbly flow (x axis in m)*

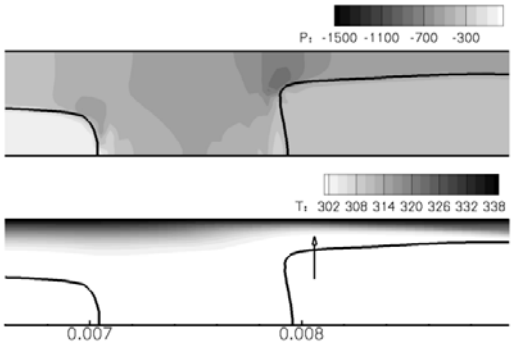

Figure 4: *Pressure and temperature isocontours at break-up point in the slug flow (x axis in m)*

Note, too, that the front slug is somewhat more elongated than the upstream ones; because it merges with the initial slug. The scenario is pretty similar to turbulent flows, where eddies randomly wash the wall-adjacent layer, transferring low-momentum fluid to the bulk, and thus heat. In this case the mechanism is rather coherent and is controlled by the frequency of slugs through the pipe.

The fluid dynamics mechanisms affecting the wall thermal layer in this area of the bubbly flow can be explained by inspecting Fig. 3, depicting the pressure and temperature isocontours at an advanced time of simulation. The upper panel shows a strong radial pressure gradient building up at the break-up location. The wall thermal layer shown in the lower panel indicates that this has been compressed by the pressure gradient after fragmentation ($x/D > 5$), yielding a higher temperature gradient from the wall. Only far downstream ($x/D = 27$) when the flow is fully developed (Fig. 5) the heat penetrates deeply the core flow. The same mechanism is observed now in the slug flow regime, where again the break-up of the flow into slugs can clearly be seen to be associated with a significant radial pressure gradient (Fig. 4). A further vigorous compression occurs at the location washed out by the rear area of the second slug (indicated by an arrow). The intensity of the radial pressure gradient is somewhat weaker than in the bubbly flow, because the distance between slugs is larger than between bubbles. The immediate consequence of this phenomenon is the sudden compression of the thermal layer against the wall, which in turn promotes locally the radial gradient of temperature. This increase in the thermal gradient is the precursor for promoting heat transfer along the pipe. Figure 5 presents a bubbly flow scenario taken where the centre of the selected cell is located around $x/D = 27$, in the fully developed region. Although the wall thermal layer does not seem to be affected by the cell, or slightly at the early stage of the train, the results of the heat transfer rates discussed later indicate the contrary.

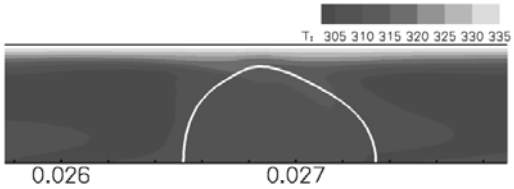

Figure 5: *Heat penetration around a bubble*

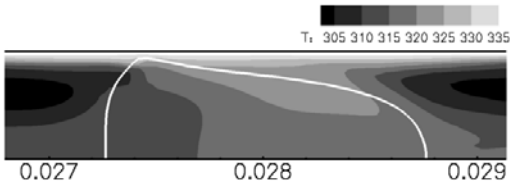

Figure 6: *Heat penetration around a slug*

Compared to the slug-flow regime results shown in the next figure, the heat penetration in the bubble core flow is less pronounced, which is well illustrated in the figures comparing temperature profiles. The difference between heat penetrations into the bulk represents about 20% of the total subcooling rate. The thickness of the wall thermal layer remains smaller than in the slug flow, as if it were permanently controlled by the fragmentation-induced pressure gradient occurring upstream. These mechanistic behaviours of the heat convection and fluid flow are corroborated with the detailed plots of thermal flow profiles and Nusselt number distribution presented in the next section. Figure 6 displays now a post-fragmentation sequence of the slug flow taken in the fully developed region, where the centre of the selected cell is at about x/D = 28. This zone has indeed reached fully-developed steady-state conditions. The heat diffuses first from the wall down starting from the front surface of the slug. As the slug grows in scale and expands closer to the wall, the heat is driven from the large-curvature back circumference. But the main heat removal mechanism is seen to be essentially a convective transport taking place at the back of the slug, where large-curvature surfaces approach the wall. A jet-like flow forms there and penetrates the cell, transporting heat into the core. The heat gradually penetrates the entire slug in this way.

4. Thermal-flow profiles

The two-phase velocity and heat profiles around individual bubbly cells are compared in Fig. 7 to the corresponding single-phase flow ones. Labels 1, 2, 3 and 4 stand respectively for: (1) in the wake of the cell, (2) and (3) in the core of the cell, and (4) upstream the cell. These profiles ahead (4) and in the wakes (1) of bubbles and slugs are very much similar to single-phase axisymmetric profiles, whereas within the cells (at stations 2 and 3) the flow is subject to substantial overturning. In the bubbly flow case the analysis of the data indicates that the flow in stations 1 and 4 (in the wake and ahead) is not affected by the presence of the bubbles, unlike in the cell core (at stations 2 and 3) where a recirculation is clearly taking place in the front part. The slopes of the corresponding thermal field profiles show an interesting behaviour: at all the stations the slopes are clearly sharper than in the single-phase flow taken at the same location – in the water flow the thermal wall layer develops fully only at x/D = 70--, meaning that the heat transfer should be larger. In contrast to the velocity field then, the heat profiles at locations 1 and 4 deviate from the single phase, suggesting that it is the velocity profiles that are repeatedly affected by the cells (at stations 2 and 3) that prevent the wall thermal layer to naturally develop along the pipe. It is also interesting to note that the scalar penetration from the wall is maximal within the cell core. We are thus facing a new situation where the Reynolds analogy does not hold any longer. The profiles around the slug cell are compared in Fig. 8. The behaviour observed for the bubbly flow can be noticed here, too. The velocity profiles deviate from the corresponding single-phase results only slightly in the wake and ahead of the cell, whereas the structure inside the slug exhibits a reverse flow tending to trap heat longer within the cell. The backflow is more intense than in the bubbly regime (-3 m/s as compared to -2 m/s), which explains why, in average, scalar penetration in the bulk is larger than in the bubbly flow.

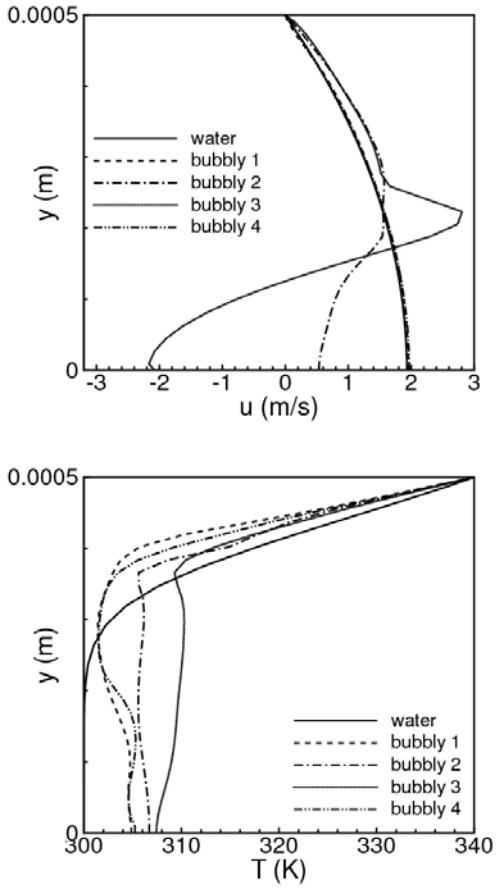

Figure 7: *Fluid and heat profiles in bubbly flow*

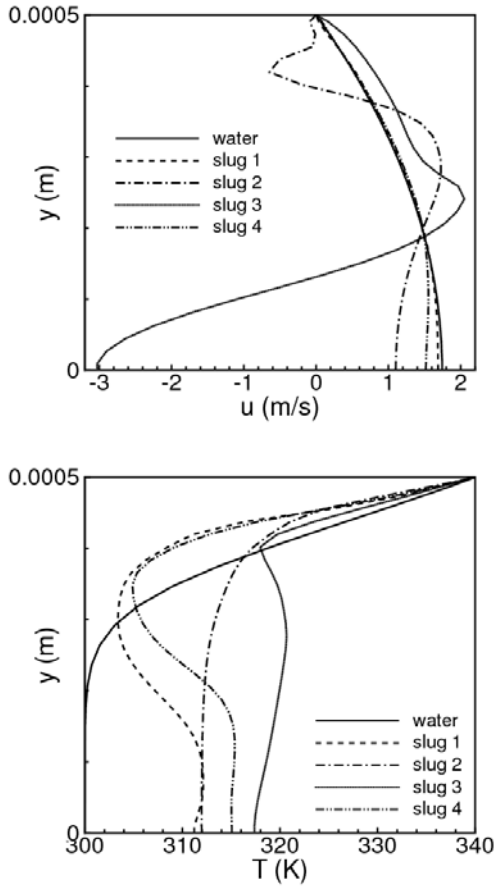

Figure 8: *Fluid and heat profiles in slug flow*

This should have little consequences though on the Nusselt number distribution, since the difference in the bulk temperature of the single and two-phase flows is not significant. The heat profiles within the wall thermal layer are again shown to present sharper slopes than the single phase. The scalar penetration inside the core is larger than in the bubbly flow, in particular at station 3 where the flow overturns.

5. Nusselt number distributions

Figures 9 and 10 present the local $\boldsymbol{Nu_x}$ and averaged Nusselt number distributions along the axis for single and two-phase flow regimes. The local Nusselt number is determined using the bulk temperature T_b defined using both the density and heat capacity as these are space and time dependent. The results obtained for the fine mesh resolution are detailed in Figs. 9 and 10 below. The water flow results depicted in both the panels corroborate with the Hagen-Poiseuille flow solution, according to which, Nu_{mean} asymptotes towards 3.67 for constant wall temperature. The water bubbly and water slug flow return slightly lower Nusselt values than the water plug (results not shown here). Turning now to the two-phase flow results, the comparison clearly reveals a substantial increase in the heat transfer rate with increasing void-inclusion length scale. The slug-train flow data show the largest fluctuations around the mean, with an RMS comparable to the slug flow, but larger than the bubbly flow. The maximum value Nu = 32 is reached for the slug-train flow regime, while for the slug it attains 25. These results are close to the measurements of Monde & Mitsutaki mentioned in [1]. The successive marked frequencies are the signature of individual slugs traversing the pipe, or more precisely their wall-adjacent, rear circumferences, as discussed previously.

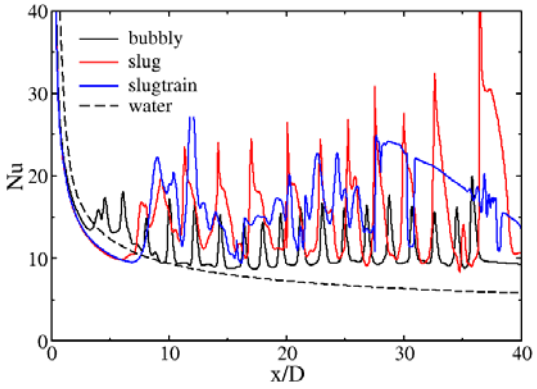

Figure 9 : *Nusselt number distribution*

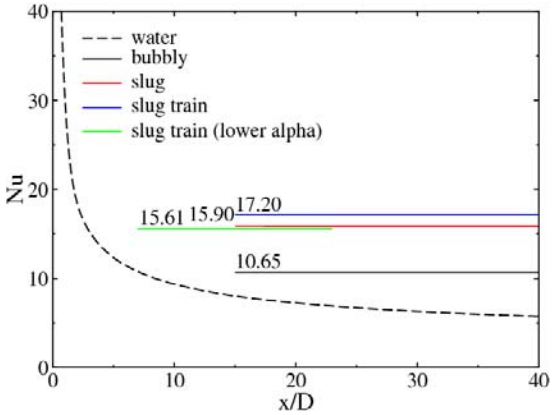

Figure 10 : *Average Nusselt number distribution*

The average values presented in Fig. 10 indicate that for the slug-train and slug flows, the data asymptote towards Nu_{mean}= 17.2 and 15.95, respectively, which is four times larger than in single phase. Lower but coherent fluctuations around the mean value Nu_{mean}= 10.65 are observed in the bubbly flow, with marked peaks corresponding to the liquid zones squeezed between the bubbles and the wall. The average Nusselt number is three-to-four times higher in the two-phase flow, but the slug and slug-train flows remove more heat due to the large blockage effect exerted, and to the background fluctuating flow induced as discussed previously. Detailed analysis of the results is available in the companion paper [6].

6. Conclusion

Detailed computational microfluidics flow simulations have been performed to study the effect of varying flow regime on the heat transfer in small tubes. Interface tracking methods were employed for the purpose, providing local detailed information about heat transfer and fluid flow. Overall the heat removal rate in two-phase flow is higher than in single phase. Subtle differences were revealed between slug flow, which dissipates more heat in the bulk, and bubbly flow, which has a higher wall heat flux due a pronounced blockage effect. It is in particular shown that the wall thermal layer thickness acting as a resistor is controlled by the pressure induced by early train dislocation into slugs or bubbles. This confinement effect is shown to influence heat transfer, which is higher in the bubbly flow than in the slug flow.

References

[1] P. Ua-Arayaporn, K. Fugakata, N. Kasagi and T. Himeno, Numerical simulation of gas-liquid two-phase convective heat transfer in a microtube. *Proc. ECI I. Conf. Heat transfer and Fluid Flow in Microscale*, Castelvecchio Pascoli, Italy, Sep. 25-30, 2005.

[2] M. Sussman, P. Smereka and S. Osher, A Level set approach for computing incompressible two-phase flow. *J. Comp. Physic*s, 114, (1994), 146-167.

[3] D. Lakehal, M. Meier and M. Fulgosi, Interface tracking for the prediction of interfacial dynamics and heat/mass transfer in multiphase flows , *Int. J. Heat & Fluid Flow*, 23, (2002) , 242-257.

[4] H.M. Friess and D. Lakehal, A New method for including surface tension and contact angle dynamics in the simulation of two-Phase flow. *Proc. CHT04*, Kirkenes, Norway, April, 2004.

[5] W.L. Chen, M.C. Twu and C. Pan, Gas-liquid two-phase flow in microchannels. *Int. J. Multiphase Flow*, 28, (2002), 1235-1255.

[6] D. Lakehal, G. Larrignon and C. Narayanan, Computational heat transfer and two-phase flow in miniature pipes, in press, *J. Microfluidics & Nanofluidic*s, 2007.

[7] TransAT© User Manual: www.ascomp.ch